# Ultrasonic imaging of the group velocity surface about the cubic axis in silicon

Cite as: Journal of Applied Physics **79**, 1857 (1996); https://doi.org/10.1063/1.361086
Submitted: 15 June 1995 • Accepted: 17 November 1995 • Published Online: 04 June 1998

**Kwang Yul Kim, Kathleen C. Bretz, Arthur G. Every, et al.**

# Ultrasonic imaging of the group velocity surface about the cubic axis in silicon

Kwang Yul Kim,[a] Kathleen C. Bretz, Arthur G. Every,[b] and Wolfgang Sachse
*Department of Theoretical and Applied Mechanics, Thurston Hall, Cornell University, Ithaca, New York 14853*

(Received 15 June 1995; accepted for publication 17 November 1995)

This article reports measurements of the group velocity surface of silicon in the region of the ⟨100⟩ axis. Pulsed ultrasonic beams generated by a piezoelectric longitudinal mode transducer are transmitted through water and focused onto a small spot on the surface of a (001) oriented silicon single crystal disk. This gives rise to transient elastic waves which propagate in a wide range of directions through the specimen and they are detected by a small piezoelectric longitudinal mode transducer fixed at the center of the opposite face. The imaging of the group velocity surface about the ⟨100⟩ axis is accomplished by scanning the focused beam in various directions along lines that intersect at epicenter. The scanned images reveal complex foldings of the slow transverse sheet of the ray surface about the ⟨100⟩ axis, in general agreement with the predictions of ray acoustics. However, the observed image manifests pronounced wave motions well beyond the cuspidal edges predicted by ray acoustics. This phantomlike feature or eidolon can be explained on the basis of diffraction resulting from the finite wavelength of the ultrasonic waves.  [S0021-8979(96)07104-4]

## I. INTRODUCTION

In the treatment of wave propagation in elastically anisotropic solids, extensive use is made of four representative surfaces:[1,2] the phase velocity surface, the slowness or inverse phase velocity surface, the ray or group velocity surface, and the inverse group velocity surface. The phase velocity surface conveys an impression of the directional dependence of the longitudinal and shear stiffnesses. From a knowledge of the tensor elastic constants and density of a medium, this surface is easily calculated by solving the Christoffel equation as a function of the wave normal **n**. The Christoffel secular equation is cubic in $\nu^2$ where $\nu$ is the phase velocity, and this yields a surface of three sheets corresponding to the quasi-longitudinal (QL) and two quasi-transverse (QT) modes. From an analytical point of view, the slowness surface is the most important of the acoustic surfaces, being fundamental in the treatment of surface acoustic waves and plate modes, reflection and refraction at boundaries, focusing and other phenomena. Christoffel's secular equation can be cast in the form of a sextic equation for the slowness **s**, and this forms the basis of much of the analysis. There are no general expressions available for the ray and group slowness surfaces. It can be shown that the equation of the ray surface in the most general case[3] could be of degree as high as 150. Not surprisingly, for many anisotropic media the ray surface has a fairly complex topology, with the outer QT branches being folded in various ways. The group slowness surface has a similar topology, but inverted with respect to distance from the origin. Usually the ray or group slowness surface is constructed by Monte Carlo methods,[4–6] starting with a random distribution of wave normals. Ironically it is the ray and group slowness surfaces that are the physically most real of the acoustic surfaces and the most readily visualized experimentally.

For a number of years phonon imaging at liquid helium temperatures has provided graphic insight into the topology of the ray surfaces of many crystals.[6] These images contain complex patterns of caustics, which are the projection of the folded edges of the ray surface on the imaging plane. The heat pulses that make up a phonon image display in their time dependence separate peaks for the individual sheets of the ray surface (not always resolvable), and the arrival times of these peaks give the scale of the ray and group slowness surfaces. Phonon imaging, because of the high frequencies of the thermal phonons employed [typically $(1–10)\times10^{11}$ Hz], is essentially a far-field phenomenon, and it is sufficient to treat the phonons as small wave packets that travel through the medium at their group velocity $V_g$. Hence, at any instant these phonons lie on the wave surface, which is the group velocity surface scaled by a factor of time $t$.

Recently a number of ultrasonic experiments have been carried out that simulate pointlike excitation and detection, using techniques such as capillary fracture, laser thermoacoustic excitation and interferometric detection, small aperture piezoelectric transducers, capacitive detectors, and scanning acoustic microscopy,[7–13] etc. In some of these experiments tone bursts are used with the detected signals interpreted in the frequency domain, while in other experiments step or $\delta$-function forces are used and the detected signals are interpreted in the time domain. The ultrasonic images generated using frequency domain methods preserve the broad overall features of the focusing patterns predicted on the basis of ray acoustics, but the finer features are lost. Instead there is a pattern of diffraction fringes which are most evident in the vicinity of the geometrical caustics where the effects of diffraction broadening are most pronounced.[13,14] The fringes can be interpreted as arising

[a]Electronic mail: Kykim@msc.cornell.edu
[b]Department of Physics, University of the Witwatersrand, P. O. Wits 2050, Johannesburg, South Africa.

from interference between different sheets of the wave surface which meet at a fold edge. This has been termed internal diffraction by Hauser *et al.*[8] and Weaver *et al.*[9] Wave theory also predicts that the intensity does not drop suddenly beyond a cuspidal edge but falls off gradually (see, e.g., Pearcey[15]), more so as the frequency is decreased. These effects have been observed experimentally by Hauser *et al.*,[8] Weaver *et al.*,[9] Wesner *et al.*,[10] and Kim *et al.*[13]

In these frequency domain experiments information about the ray surface is concealed in a convoluted form in the diffraction pattern. Time domain experiments, on the other hand, yield an explicit visualization of the ray surface. The response of a solid to a point force having a step or $\delta$-function time dependence consists of a continuous wave interspersed with singular features such as kinks, discontinuities and divergences which are known as wave arrival singularities, and which travel outwards from the point of excitation at a group velocity in each direction; these singularities at any instant lie on the wave surface.[3] Wave arrivals have been observed by Every and Sachse[16] in laser generated ultrasound experiments on silicon, and more recently in extensive experiments by Kim *et al.*[17,18] A detailed exposition of the different types of wave arrival singularities and a comparison between theory and experiment for zinc and silicon single crystals has been given by Every and Kim.[19] Interalia, they have pointed out that beyond a cuspidal edge the wave arrival singularities are replaced by a quasi-singular feature that persists for some distance, becoming gradually broadened. We term this feature an *eidolon*, connoting a phantomlike trace of a singular feature and tracing its etymology in Greek.

The Monte Carlo simulated ray surface of silicon exhibits a complex folding of the QT sheets in the vicinity of the $\langle 100\rangle$ directions.[18] In this article we report a detailed experimental study of the ray surface of silicon based on scanning an ultrasonic beam focused on the surface of a (001) oriented silicon disk in various directions. The waves are detected with a small aperture longitudinal mode piezoelectric transducer fixed at the center of the opposite face of the specimen. These scan images clearly reveal the complicated fold structure of the ray surface of silicon near the [001] axis. By combining the scan images obtained in various directions between zero and 45° measured from the [100] direction on the surface, one can construct a 3D image of the ray surface, which generally conforms to the prediction of ray acoustics. However, because of the finite wavelength of the ultrasonic waves, sharp features predicted on the basis of ray acoustics are modified by diffraction, which is particularly pronounced in the region of cuspidal edges. The most striking feature is the persistence of a signal beyond the cuspidal edge, which could easily be mistaken for a wave arrival, and which, as mentioned above, we describe with the term eidolon. The eidolon is observed to be particularly pronounced close to the $\langle 110\rangle$ directions. In the following we will investigate these features in detail.

## II. THEORETICAL ASPECT

### A. Geometric acoustics

From a geometrical acoustics point of view, the ray surface of an elastically anisotropic solid is considered the locus of all group velocity vectors $V_g$. Scaled by a factor of time $t$ this is the wave surface on which acoustic energy released as a short burst from a point source at the origin spreads outwards. The wave surface is useful, for instance, in describing how a ballistic heat pulse spreads outwards in a crystal. The ray or group velocity $V_g$ is obtained from the relation[1,2]

$$V_g \equiv \nabla_k \omega = \nabla_n V = -\frac{\nabla_s \Lambda}{s \cdot \nabla_s \Lambda}, \tag{1}$$

where $\omega$ is the angular frequency, $\mathbf{k}$ the wave vector, $\mathbf{n}=\mathbf{k}/k$ the wave normal, $V$ the phase velocity, $s=\mathbf{n}/V=\mathbf{k}/\omega$ the slowness, and $\Lambda$ the equation of slowness surface given by

$$\Lambda = \det|C_{ijkl} S_j s_l - \rho \delta_{ik}| = 0. \tag{2}$$

In the above equation $C_{ijkl}$ and $\rho$ denote, respectively, the elastic constant and density of a medium and $\delta_{ik}$ the Kronecker's delta.

Equation (1) indicates that the direction of group velocity at a point of the slowness surface is normal to the slowness surface at that point. Understanding the topography of the slowness surface is very important for mapping out the ray surface. The slowness surface given by Eq. (2), also known as the refraction or index surface, is of degree six in $\mathbf{s}$ and consists of three sheets. For the cubic symmetry of a silicon specimen, the three sheets remain separated except along the fourfold symmetry axes $\langle 100\rangle$ where the transverse sheets make smooth contact and along the threefold symmetry axes $\langle 111\rangle$ where the transverse sheets meet at a conical point.[1] Except for certain rare materials, the innermost sheet, known as the QL surface, is completely separated from the other two transverse sheets. It remains entirely convex, and its sheet of the ray surface is therefore not folded at all.[3] The QL mode, having the highest group velocity, arrives first at a detector and can be easily and unambiguously identified in the detected signal.

The shapes of the fast transverse (FT) slowness and group velocity sheets of silicon have been described by Hurley and Wolfe.[5] This ray sheet is absent in the images obtained in our experiment for the following reasons. The polarization pattern of the FT branch[13,16] is such that these modes are almost perfectly shear horizontal (SH). Since the focused ultrasonic beam impinging on the silicon surface is axisymmetric, these modes are not generated to any extent. Moreover, the $L$ mode piezoelectric transducer used in our experiment detects the component of motion normal to the surface of a specimen and would not detect these modes, even if present. We will therefore not discuss the FT modes further.

With regard to the slow transverse (ST) mode, the topography of its sheets of the slowness surface is described in Refs. 4 and 5 and its mapping onto the ray surface is discussed in detail by Every.[4] A projected view of the slowness surface near the [100] axis is displayed in Fig. 1(a). The fairly wide furrows (shaded area) joining around the $\langle 100\rangle$

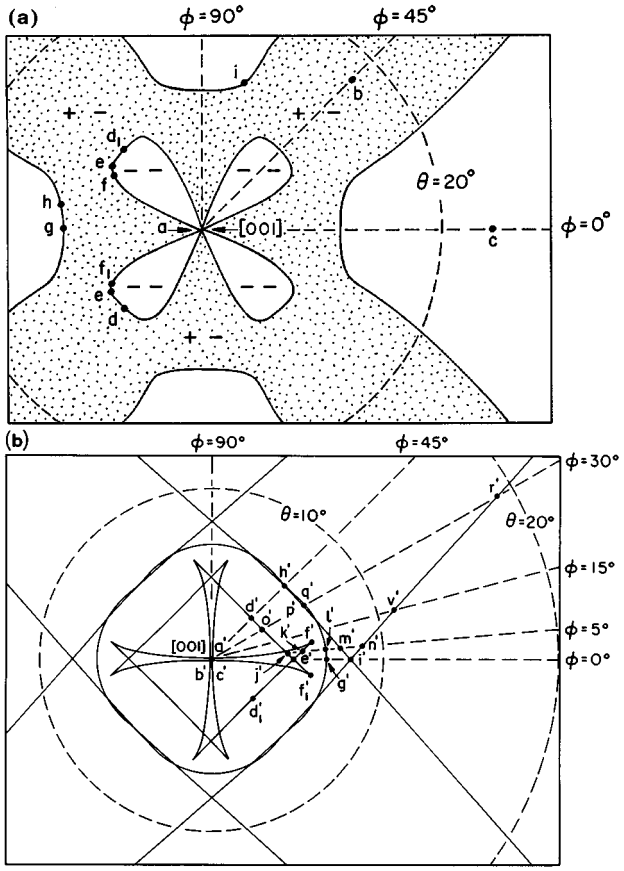


FIG. 1. Polar plots of: (a) the ST mode slowness surface of silicon about the [001] axis, where the positive/negative Gaussian curvatures are indicated by $+/-$ signs, and (b) disposition of folds of silicon near the [001] direction.

axis are saddle-shaped with the negative Gaussian curvature. The small white cloverleaf shaped regions directly around each ⟨100⟩ direction are concave with both principal curvatures being negative. Elsewhere are white convex regions with both principal curvatures being positive. The disposition of folds in the ray surface near the [001] direction is shown in Fig. 1(b), where the points corresponding to those of Fig. 1(a) are marked with the same but primed letters. Fig. 1(b) is very similar to the images of phonon caustics of silicon which have been observed at cryogenic temperatures.[20] The elastic constants $C_{ij}$ and density $\rho$ of silicon used to generate these figures are: $C_{11}=165.8$ GPa, $C_{12}=63.9$ GPa, $C_{44}=79.6$ GPa, and $\rho=2331$ kg/m$^3$ and are taken from Ref. 21.

The normal at the point $a$ and also the normals at the points $b$ and $c$ lying, respectively, on the (110) and (010) planes of the slowness surface shown in Fig. 1(a) are all parallel to the [001] direction. The magnitudes of the associated group velocities, which are parallel to the [001], are in the order $V_g(a)>V_g(b)>V_g(c)$. The points $a$ in Fig. 1(a) and $a'$ in Fig. 1(b) are those of tangential degeneracy, where the FT and ST slowness (and ray) sheets make tangential contact with each other. Therefore, one would expect to find four rays emanating from a point source and propagating in the ⟨001⟩ direction, one longitudinal and three transverse modes. This feature is apparent in the [001] direction in Figs. 2(a)–2(e), which show the predicted wave arrivals for a silicon specimen of thickness=49.15 mm. The points $g$ and $d$ in Fig. 1(a) are the inflection points where the principal curvature in the symmetry plane is zero. The group velocities and their $\theta$ angles, which correspond to these points and to the points $a,b$, and $c$ lying in the symmetry planes in Fig. 1(a), can be analytically calculated using the formulas derived by Kim *et al.*[22,23] Those of other points lying in nonsymmetry planes in Fig. 1(b) have been numerically obtained by the aforementioned Monte Carlo method.

Referring to Fig. 1(b), the various group velocity sections for constant polar angle $\phi$ that lie between the (010) and (110) planes are indicated by the straight broken lines that pass through the [001] pole. The points of cuspidal edges in Figs. 2(a)–2(e) are the mapped images of the corresponding points where the broken line intersects with the solid line in Fig. 1(b). They are marked with the double-primed same letters in Figs. 2(a)–2(e). The cusp of the maltese cross denoted by $f'$ lies in the direction of polar angle $\phi$ approximately equal to 10°. A group velocity section lying within the maltese cross exhibits the most complicated fold structures except for the symmetry section (010) of $\phi=0°$, which indicates three ST mode folds. For example, the section of $\phi=5°$ has five folds, the two innermost branches of which close to the [001] direction with the cuspidal edges marked by $j''$ and $k''$ lie so close to each other that they are not well resolved in Fig. 2(b). The cusp edge $j''$ has a cone angle $\theta$ of about 4.5° measured down from the [001] direction. With a broadband pointlike source which can generate all the modes, one would theoretically expect and, in an ideally well-resolved experiment, observe a total of 13 rays consisting of one QL, one FT, and eleven ST modes propagating in the region whose cone angle is less than 4.5°. There are four folds in a ray section whose polar angle $\phi$ lies between 10° and 45°, as shown in Figs. 2(c) and 2(d). The (110) ST mode group velocity section of $\phi=45°$ shown in Fig. (2e) shows two folds near the [001] direction. Its FT section and one of its ST branches meet at the circle of internal conical refraction that centers at the [111] direction.

### B. Wave theory

Although the group velocity sections of Figs. 2(a)–2(e) generally conform to the corresponding group velocity surfaces observed and described in Sec. IV, the far-field condition that the source-to-detector distance is much greater than a typical wavelength involved, is not very well satisfied in the MHz ultrasonic frequency range in which a typical wavelength is of order of mm. As a result, the ray surface has to be considered in the context of wave theory. Various rays having differing wave normals interfere and this interference is most pronounced in the cuspidal regions where the rays are more closely clustered. Also, beyond the predicted cuspidal edge of the ray surface, one observes for some distance the continuation of a feature that looks like and might be misconstrued as a wave arrival, and which we term an eidolon. This is not a geometrical acoustics effect, and to understand it one needs to adopt a more fundamental approach which takes into account diffraction effects.

The displacement response of an infinite, elastically anisotropic continuum subjected at the origin to a point force with Heaviside step function time-dependence

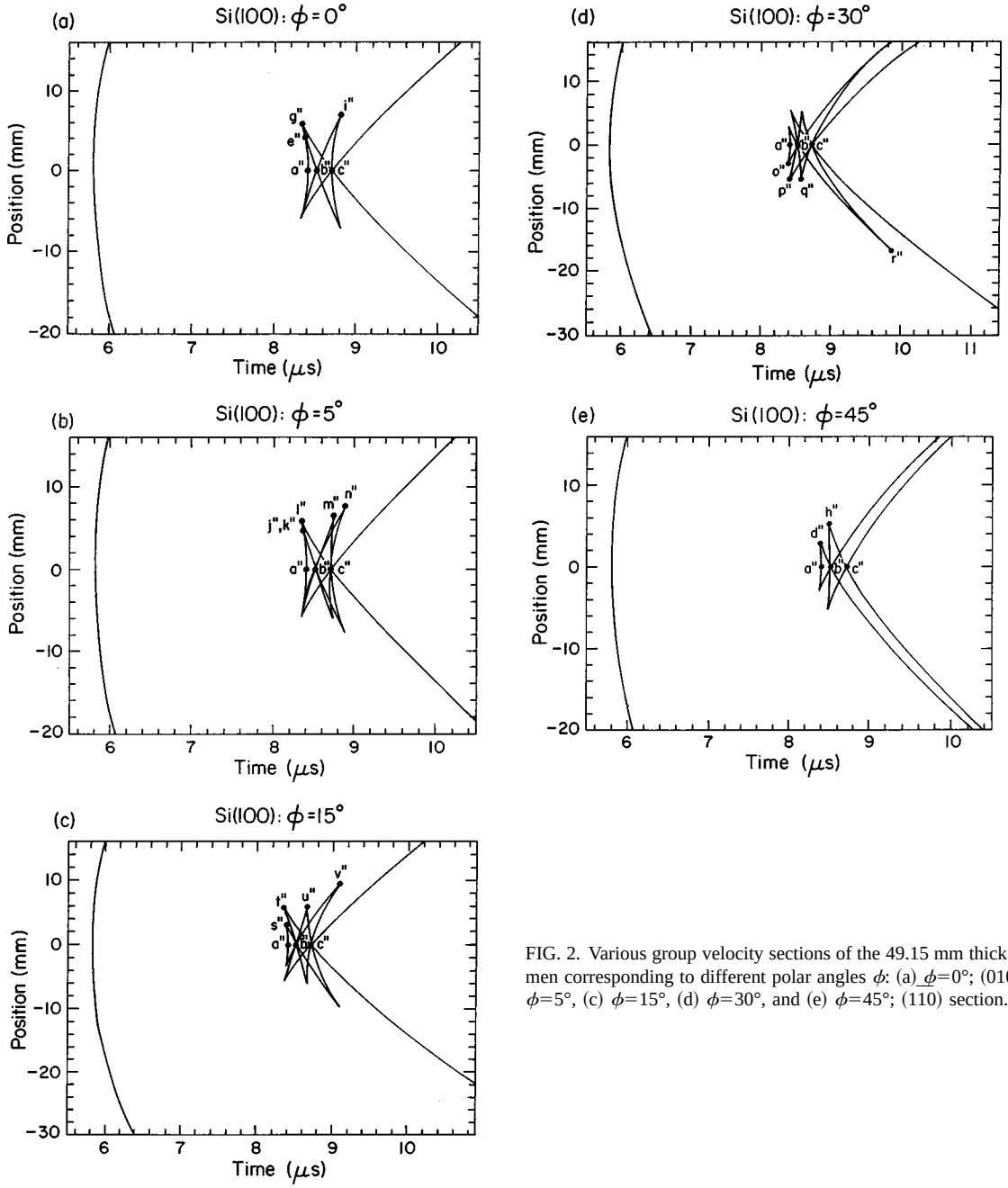


FIG. 2. Various group velocity sections of the 49.15 mm thick silicon specimen corresponding to different polar angles $\phi$: (a) $\phi$=0°; (010) section, (b) $\phi$=5°, (c) $\phi$=15°, (d) $\phi$=30°, and (e) $\phi$=45°; (110) section.

$$\Theta(t)=\begin{cases}0, & t<0\\ 1, & t>0\end{cases} \tag{3}$$

can be expressed in the form (Every and Kim[19])

$$\tilde{G}_{sp}(\mathbf{x},t)=\sum_{j=1}^{3}\left\{\frac{-1}{8\pi^2\rho}\int_{\Omega} d\Omega\; s^{(j)^3}\Lambda_{sp}^{(j)}\delta(t-\mathbf{s}^{(j)}\cdot\mathbf{x})+\frac{\Theta(t)}{8\pi^2\rho x}\int_0^{2x} d\phi\; s^{(j)^2}\Lambda_{sp}^{(j)}\right\}, \tag{4}$$

where $s$ and $p$ refer to the sensing and forcing directions, respectively; sum is over the three acoustic branches; $\Lambda_{sp}^{(j)}=U_s^{(j)}U_p^{(j)}$ depends on the projection of the polarization vector $\mathbf{U}^{(j)}$ for each mode $j$ on the sensing and forcing directions; $d\Omega$ is the element of solid angle in which the slowness $s^{(j)}$ lies and which is integrated over the hemisphere centered on the viewing direction $\mathbf{x}$. The second integral is a line integral around the periphery of this hemisphere.

Wave arrival singularities in the displacement response arise from integration over points on the slowness surface where $\mathbf{s}^{(j)}\cdot\mathbf{x}$ is stationary, i.e., where the normal to the slowness surface or group velocity points in the direction of $\mathbf{x}$. For generic points on the slowness surface, it can be shown, using the stationary phase approximation, that the singularity takes the form of a discontinuity where the principal curvature $K_1$ and $K_2$ of the slowness surface are both positive (convex) or negative (concave) and of a logarithmic singularity where one principal curvature is positive and the other negative (saddle shaped). In both cases there is a multiplica-

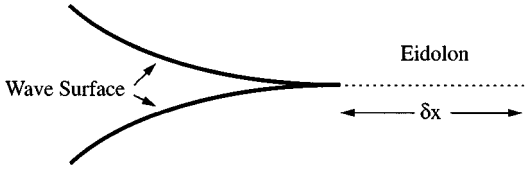


FIG. 3. Schematics of a cusp as a function of distance $\delta x$ from the cusp edge.

tive factor $1/\sqrt{|K_1K_2|}$ which diverges on approach to the cuspidal edge where the wave arrivals meet. Precisely at the cuspidal edge there is a single arrival displaying a $|t|^{-1/2}$ divergence.

Beyond the cuspidal edge there is no wave arrival in the strict sense. Nevertheless, because of diffraction, there is a deep minimum to the response function along the common tangent at the cuspidal edge (see Fig. 3) falling off as $(\delta x)^{-1/4}$, where $\delta x$ is the distance from the cuspidal edge. This type of quasi-singular feature, which is an eidolon, is a fairly common occurrence in both calculated and measured response functions of anisotropic solids.

Measured wave arrivals always display a certain amount of rounding because of the finite rise time and spatial extent of the source and the finite bandwidth of the associated electronics. As a result, the fact that the measured response within and near the cuspidal edge where the two wave arrivals interact and can no longer be resolved is not dissimilar in appearance to that of the eidolon beyond the cuspidal edge. The eidolon could thus mistakenly be interpreted as an extension of the wave surface beyond the fold edge. This eidolon feature is to be seen in the results of a number of articles (e.g., A. A. Kolomenskii and A. A. Maznev[24] on laser generated surface acoustic wave (SAW) on crystals; M. Veidt and W. Sachse[25] on laser generated plate modes in a graphite/epoxy laminate; Corbel *et al.*[26] on laser generated waves in a fiber composite plate) but it has not been widely commented on before.

## III. EXPERIMENTAL METHOD

In our scan-imaging experiment, we perform measurements with a (001)-oriented silicon crystal disk of thickness

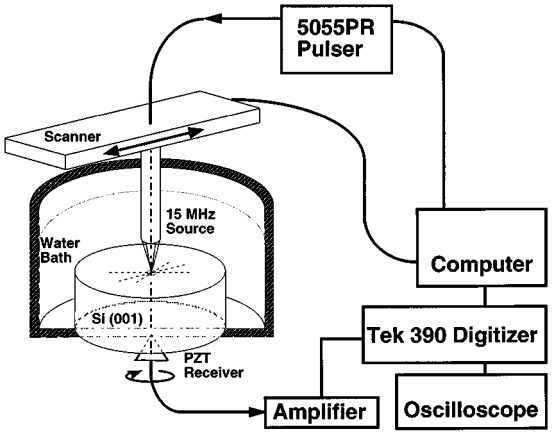


FIG. 4. Experimental setup and electronic block diagram.

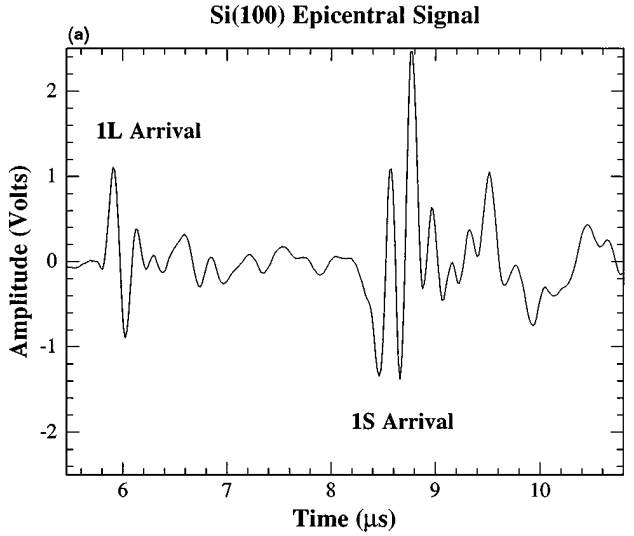


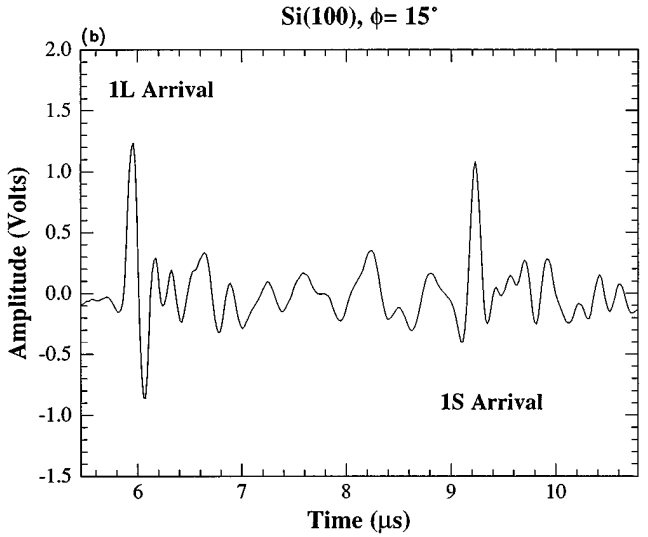


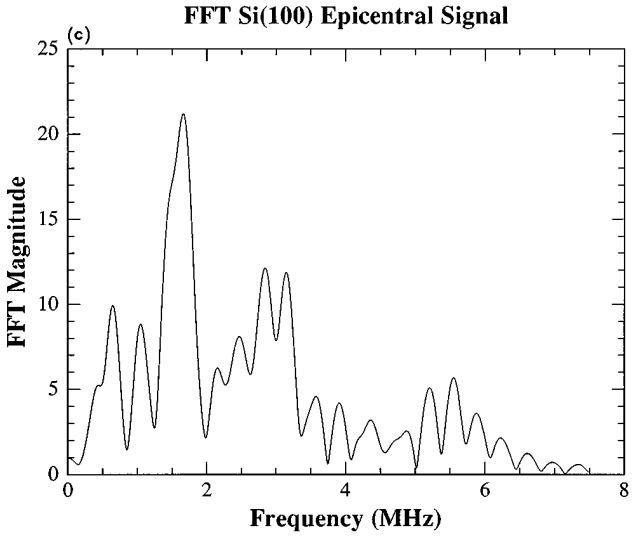


FIG. 5. Typical signals detected by the L mode PZT detector at (a) epicenter and (b) an off-epicentral position ($\phi$=15°, $\theta$=15°), and (c) FFT magnitude spectrum of the epicentral signal in (a).

49.15 mm and diameter 100 mm. The top and bottom (001) planes of the silicon specimen are polished parallel to each other. The specimen and a source transducer are submerged in a water bath mounted on a rotating stage, as shown in Fig.

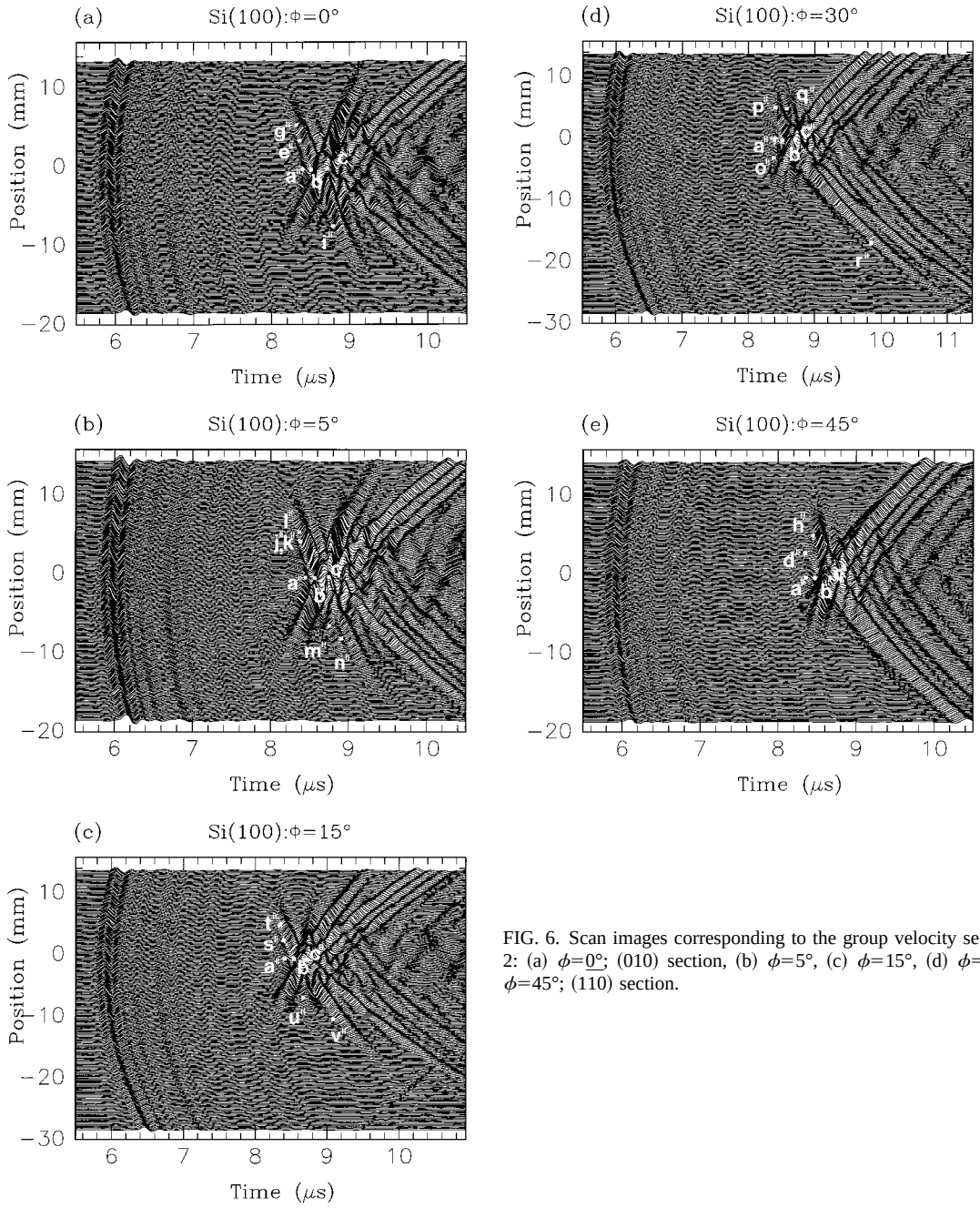


FIG. 6. Scan images corresponding to the group velocity sections in Fig. 2: (a) $\phi$=0°; (010) section, (b) $\phi$=5°, (c) $\phi$=15°, (d) $\phi$=30°, and (e) $\phi$=45°; (110) section.

4, which also shows a scanning and detecting electronic block diagram. The source transducer has a 15 MHz bandwidth and a 25 mm focal length, and is a 1/2 inch diameter longitudinal (L) mode transducer of immersion-type, which is attached to an $x$-$y$ scanner and also connected to a pulser. The transducer generates a sharp transient pulse which is focused on the top surface of the silicon specimen. The focusing diameter is about 0.2 mm, when excitated by the high-voltage pulse derived from the pulser. The ultrasonic waves that transmit via water and focus on the specimen surface act as a pointlike axisymmetric source, which generates a broadband ultrasonic elastic pulse propagating in a wide range of directions through the specimen.

The specimen is fixed at the bottom of the water bath with a detecting transducer attached at the center of the bottom surface of the specimen. The detector is a L mode piezoelectric $Pb(Zr,Ti)O_3$ (PZT) transducer of diameter 1.3 mm. A scanning is performed in steps of 0.1 mm in a linear fashion that crosses the epicentral spot and extends an equal distance of 25 mm on both sides of the epicenter. This covers a conical angle of $2\theta = 2\tan^{-1}(25/49.15) = 54°$. The detected signal is amplified with 40 dB gain and digitized with a 10 bit resolution at a 60 MHz sampling rate. The digitized signals are displayed on an $x$-$y$ oscilloscope and brought into a microcomputer which stores them for image construction. The pulsing of a source, data acquisition, and scanning are performed in steps following the computer-controlled instructions. After the scanning is finished in one direction, the specimen is rotated about the [001] epicentral direction to scan in another direction in a 5° incremental step. Because the (001) silicon crystal possesses a repetitive pattern of 45° period, the scanning direction is confined in a polar angle $\phi$ of 45° measured from the [100] toward the [110] direction lying in the (001) plane.

## IV. SCAN IMAGE

Figures 5(a) and 5(b) display, respectively, an epicentral signal and a typical off-epicentral signal at the point of $\phi=15°$ and $\theta=15°$, which are both detected by the small piezoelectric transducer. In Figs. 5(a) and 5(b) 1L and 1S denote the first longitudinal and shear (transverse) mode arrivals, respectively. The fast Fourier transform (FFT) magnitude spectrum of the epicentral signal is shown in Fig. 5(c). The first arrival above the noise level corresponds to that of the QL mode, after which it is seen for ringing of the signal to persist for a while and then the signal becomes so complicated that it is very difficult to identify the arrivals of other modes. The identification of other mode arrivals can be facilitated by constructing the scan images, which are shown in Figs. 6(a)–6(e). The first arrivals of the QL and slow transverse modes are marked with 1L and 1S in Figs. 5(a) and 5(b), respectively. Three transverse ray arrivals in the [001] epicentral direction are marked in Figs. 6(a)–6(e) with $a''$, $b''$, and $c''$, each corresponding to the points of the same letters in Figs. 1 and 2. The cuspidal edges in Fig. 2, which are determined from ray theory, are also marked in Fig. 6, where the same letters indicate the same cuspidal edges. Both Figs. 2 and 6 are drawn in the same scale for direct comparison.

It is seen in all scan images of Fig. 6 that two branches terminating at the same cuspidal edge in Fig. 2 interfere to appear effectively as one wave motion and the arrivals of the fastest ST branches in the neighborhood of the [001] direction, whose cuspidal edges lie on the fold branch $e'j'o'd'$ in Fig. 1(b), cause a small downward motion. In the $\phi=5°$ scan image of Fig. 6(b), four branches that terminate at either fold $j'$ or $k'$ of the maltese cross shown in Fig. 1(b), arrive almost simultaneously, so that they merge together as one downward motion. Immediately trailing near the [001] direction behind these wave motions are two branches that merged together with the cuspidal edges corresponding to the folds lying on the branch $g'l'q'h'$ in Fig. 1(b). The group velocities near and beyond the cuspidal edges $g''$, $l''$, and $t''$ in Figs. 6(a)–6(c) are significantly larger than those of the near-epicentral rays with the cuspidal edges $e''$, $j''$, $k''$, and $s''$. Consequently it is seen in Figs. 6(a)–6(c) that they arrive earlier than the near-epicentral rays, despite the fact that they travel longer distances. Note that the cuspidal edges of $t''$ and $u''$ in Fig. 6(c) and $p''$ and $q''$ in Fig. 6(d) have almost identical cone angles $\theta$, but the magnitudes of their group velocities are so different from each other that their arrivals are well separated in the figures.

Although comparison between Fig. 2 and Fig. 6 shows an overall approximate conformity of the ultrasonic wave surfaces to predictions of ray theory, one can immediately notice a striking difference between them. That is, the wave motions persist well beyond the cuspidal edge determined from ray acoustics in the direction of an extended cusp. This is the eidolon feature discussed in the previous section. Even though there is no true wave arrival here, there is a deep minimum to the response function which persists for some distance beyond the cuspidal edge, becoming gradually shallower until eventually it is not longer recognizable. Because of the limited time and spatial resolution of our experiments, we have not been able to confirm the negative 1/4 power law dependence of the eidolon amplitude on $\delta x$ with any accuracy. The most we can say is that our observations are consistent with a negative exponent between 0.1 and 2.3.

## V. CONCLUSIONS

We have presented the scan images of a (001) oriented silicon crystal, which portray the various group velocity sections with complicated cusps and foldings. The images of group velocity sections generally conform to the predictions of ray theory, but they show diffraction characteristics resulting from the finite wavelength of the ultrasonic waves. The most noteworthy feature of the images is the eidolon, which resembles an extension of the ray surface beyond the cuspidal edge.

*Note added in proof:* Wolfe and Hauser[27] and Wolfe[28] have recently given a vivid exposition of wave front imaging.

## ACKNOWLEDGMENTS

K. Y. Kim, K. Bretz, and W. Sachse are grateful for the financial support from the Office of Naval Research. Use of the facilities of the Materials Science Center (MSC) at Cornell University is greatly appreciated. The MSC is funded through a grant from the National Science Foundation.

[1] M. J. P. Musgrave, *Crystal Acoustics* (Holden-Day, San Francisco, CA, 1970).
[2] B. A. Auld, *Acoustic Fields and Waves in Solids*, 2nd ed. (Krieger, Malabar, FL, 1990), Vol. 1.
[3] G. F. D. Duff, Philos. Trans. R. Soc. London, Ser. A **252**, 249 (1960).
[4] A. G. Every, Phys. Rev. B **24**, 3456 (1981).
[5] D. C. Hurley and J. P. Wolfe, Phys. Rev. B **32**, 2568 (1985).
[6] G. A. Northrop and J. P. Wolfe, in *Nonequilibrium Phonon Dynamics*, edited by W. E. Bron (Plenum, New York, 1985), p. 165.
[7] A. G. Every, W. Sachse, K. Y. Kim, and M. O. Thompson, Phys. Rev. Lett. **65**, 1446 (1990).
[8] M. R. Hauser, R. L. Weaver, and J. P. Wolfe, Phys. Rev. Lett. **68**, 2604 (1992).
[9] R. L. Weaver, M. R. Hauser, and J. P. Wolfe, Z. Phys. B **90**, 27 (1993).
[10] J. Wesner, K. U. Wurz, K. Hillmann, and W. Grill, in *7th International Conference on Phonon Scattering in Condensed Matter VII*, edited by M. Meissner and R. O. Pohl (Springer, Berlin, 1993), p. 68.
[11] K. Y. Kim, W. Sachse, and A. G. Every, Phys. Rev. Lett. **70**, 3443 (1993).
[12] K. Y. Kim, A. G. Every, and W. Sachse, Int. J. Mod. Phys. B **8**, 2327 (1994).
[13] K. Y. Kim, A. G. Every, and W. Sachse, J. Acoust. Soc. Am. **95**, 1942 (1994).
[14] H. J. Maris, Phys. Rev. B **28**, 7033 (1983).
[15] T. Pearcey, Philos. Mag. **37**, 311 (1946).
[16] A. G. Every and W. Sachse, Phys. Rev. B **44**, 6689 (1991).
[17] K. Y. Kim and W. Sachse, J. Appl. Phys. **75**, 1435 (1994).
[18] K. Y. Kim, A. G. Every, and W. Sachse, J. Acoust. Soc. Am. **93**, 1393 (1993).
[19] A. G. Every and K. Y. Kim, J. Acoust. Soc. Am. **95**, 2505 (1994).
[20] J. A. Shields and J. P. Wolfe, Z. Phys. B **75**, 11 (1989).
[21] H. J. McSkimin and P. Andreatch, Jr., J. Appl. Phys. **35**, 2161 (1964).
[22] K. Y. Kim, Phys. Rev. B **49**, 3713 (1994).
[23] K. Y. Kim, A. R. Every, and W. Sachse, Int. J. Mod. Phys. B **10**, 235 (1996).
[24] A. A. Maznev, A. A. Kolomenskii, and P. Hess, Phys. Rev. Lett. **75**, 3332 (1995).
[25] M. Veidt and W. Sachse, J. Acoust. Soc. Am. **96**, 2318 (1994).
[26] C. Corbel, F. Guillois, D. Royer, M. Fink, and R. de Mol, Ultrasonics International Conference Proceedings, 1993 (unpublished), p. 217.
[27] J. R. Wolfe and M. R. Hauser, Ann. Physik **4**, 99 (1995).
[28] J. P. Wolfe, Phys. Today **34** (September, 1995).